available at www.sciencedirect.com

ScienceDirect

journal homepage: www.elsevier.com/locate/agrformet

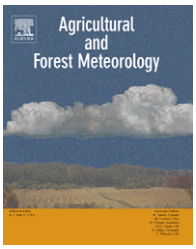

Influence of foliar density profile on canopy flow: A large-eddy simulation study

Sylvain Dupont *, *Yves Brunet*

INRA, UR1263 EPHYSE, 71 Avenue Edouard Bourlaux, F-33140 Villenave d'Ornon Cedex, France

ARTICLE INFO

Article history:
Received 30 March 2007
Received in revised form
15 January 2008
Accepted 17 January 2008

Keywords:
Coherent structures
Coriolis force
Forest morphology
Large-eddy simulation
Mixing-layer analogy
Turbulent flow
Vegetation canopy
Wavelet transform

ABSTRACT

The Advanced Regional Prediction System (ARPS) has been modified so as to simulate turbulent flow at very fine scale within and above vegetation canopies using a large-eddy simulation (LES) approach. It is first shown that this new version of ARPS is able to reproduce accurately all essential features of turbulent flow over homogeneous canopies. A sensitivity study of the flow to the morphology of the canopy, i.e. the density and vertical leaf-area (LAI) distribution, is then performed numerically over three types of canopies with five levels of leaf-area index, from 1 to 5. This study confirms the universal characteristics of turbulent flow over vegetation canopies, as previously observed from wind-tunnel and in situ experiments. It shows that the typical features of canopy flow become more pronounced as canopy density increases, and quantifies the extent to which differences in canopy morphology can explain the experimental variability observed between canopies. This variability in turbulent characteristics is mostly visible in the subcanopy space, and depends significantly on the density of the upper foliated layers. The mean longitudinal separation Λ_w between adjacent coherent structures has also been computed for each canopy using the wavelet transform and approximating the convection velocity of coherent structures as 1.8 times the average wind velocity at canopy top. Except for the sparsest canopies, the analogy between the atmospheric flow near the top of a vegetation canopy and a plane mixing layer is well verified: Λ_w is directly related to the shear length scale $L_s = U(h)/U'(h)$, where h is canopy height, U mean velocity and U' is the vertical gradient dU/dz, in a way close to the prediction $\Lambda_w/h = 8.1L_s/h$.

1. Introduction

It is now well established that turbulence over vegetation canopies is characterized by (i) a strong shear at canopy top associated with an inflection point in mean horizontal velocity, (ii) a rapid decrease of turbulent kinetic energy and momentum flux with depth in the canopy, (iii) the major role of sweep motions in momentum transfer at canopy top, and (iv) positive and negative skewnesses of the streamwise and vertical wind velocity components at canopy top, respectively, showing that turbulence is dominated by intermittent, energetic downward-moving gusts (see Finnigan, 2000, for a review).

The inflection point in the mean velocity profile at canopy top is of major importance since it is responsible for the development of large coherent eddies that control most of momentum and scalar transfer between vegetation and the atmosphere (Gao et al., 1989; Lu and Fitzjarrald, 1994). Such observations led Raupach et al. (1996) to postulate that the atmospheric flow near the top of a vegetation canopy is analogous to a plane mixing-layer flow. In both cases the development, the characteristics and length scales of coherent

* *Corresponding author*. Fax: +33 5 57 12 24 20.
E-mail address: sdupont@bordeaux.inra.fr (S. Dupont).
0168-1923/$ – see front matter
doi:10.1016/j.agrformet.2008.01.014

structures appear indeed similar. In the light of this analogy Raupach et al. (1996) deduced from many field and wind-tunnel datasets that the mean longitudinal separation Λ_w between adjacent coherent structures is a function of a shear length scale L_s (defined initially in Raupach et al., 1989, and presented further here), as for plane mixing-layer flow.

This overall behaviour of turbulent flow over plant canopies has been observed over a wide range of cases, with residual scatter that may be due to differences in canopy morphology (Raupach et al., 1986; Novak et al., 2000), i.e. plant density and vertical leaf-area distribution. Experimental studies of the influence of canopy morphology on turbulent statistical fields and coherent structures remain limited because of the difficulties in implementing such experiments (Shaw et al., 1988; Novak et al., 2000; Poggi et al., 2004). Moreover, to our knowledge no numerical investigations with detailed flow statistics have been performed so far on this matter.

The objective of the present paper is to use the large-eddy simulation (LES) technique to analyze the influence of canopy morphology on the turbulent flow and examine the validity of the mixing-layer analogy with assumptions similar to those used by Raupach et al. (1996). As LES gives access to instantaneous dynamic fields it is indeed able to simulate turbulent structures in a plant canopy larger than twice the grid mesh, whereas in the meantime subgrid-scale eddy motions are modelled.

LES over vegetation has been mostly performed with fluid mechanics models over homogeneous canopies under neutral stratification. Comparisons with field and wind-tunnel observations have provided qualitative agreement of simulated mean velocity and turbulent statistics profiles (Shaw and Schumann, 1992; Su et al., 1998). Coherent structures have also been investigated, firstly by Kanda and Hino (1994) then by Su et al. (2000) through a two-point correlation analysis, followed by Watanabe (2004) using scalar ramp detection. Over a range of atmospheric conditions, Shen and Leclerc (1997) explored the influence of instability on turbulent structures and Dwyer et al. (1997) considered the various terms of the turbulent kinetic energy budget. All these studies on homogeneous canopies demonstrated that LES is capable of reproducing in details many observed features of turbulent flow over vegetation canopies. To a lesser extent, LES has also been applied over heterogeneous vegetation canopies (Patton et al., 1998; Yang et al., 2006a, b; Dupont and Brunet, 2008, in press, s).

In the present study we use ARPS (version 5.1.5), the Advanced Regional Prediction System developed at the Center for Analysis and Prediction of Storms (CAPS) at the University of Oklahoma for the explicit prediction of convective and cold-season storms as well as weather systems at other scales. This model can be used for both large-eddy and mesoscale simulations. In the former case the integration is performed over small domains with a vertical and horizontal resolution fine enough (less than about 100 m) to resolve most boundary-layer eddies. Here, ARPS has been modified so as to simulate turbulent flows over plant canopies at very fine scales (about 2 m). To this purpose a drag force approach has been implemented in a way similar to Watanabe (2004), by adding a pressure and viscous drag force term in the momentum equation and by adding a sink term in the equations for subgrid-scale turbulent kinetic energy, so that the acceleration of the dissipation of turbulent eddies in the inertial subrange can be represented. A dry and neutral atmosphere is considered in all simulations.

After a description of the changes made to the equations of ARPS (Section 2), we show a validation of the model in a homogeneous canopy case (Section 3). A sensitivity study of the turbulent flow to the vegetation morphology is then performed over 15 canopies through the analysis of the basic turbulent statistics profiles and wind velocity correlations (Section 4). Following this, the validity of the plane mixing-layer analogy is investigated numerically in Section 5 for a range of canopy morphologies, using the wavelet transform technique. Finally, we summarize and conclude this study (Section 6).

2. Methods

2.1. *Model equations*

ARPS is a complete weather forecast system that has been extensively validated over the last decade for a variety of mesoscale flows. Here the model is extended so as to simulate turbulent flow within vegetation canopies. A brief description of the model is first presented with a focus on the implementation of the canopy. A detailed description of the standard version of the model and its validation cases are available in the ARPS User's Manual (Xue et al., 1995) and in Xue et al. (2000, 2001).

ARPS is a three-dimensional, non-hydrostatic, compressible model where Navier–Stokes equations are written in terrain-following coordinates. The grid is orthogonal in the horizontal direction and stretched in the vertical direction. The model solves the conservation equations for the three wind velocity components, pressure, potential temperature and water (water vapor, cloud water, rainwater, cloud ice, snow and graupel). Wind components and atmospheric state variables (air density, pressure and potential temperature) are split into a base state (over-barred variables) and a deviation (double-primed variables). The base state is assumed horizontally homogeneous, time invariant and hydrostatically balanced. For high spatial resolution, conservation equations are filtered to separate small and large scales. Therefore, filtered equations can be seen as grid volume-averaged equations. Within the vegetated layer, the shear flow at the canopy top involves eddies larger than those produced in the wakes behind vegetation elements, and eddy dissipation occurs through the smallest eddies (Kolmogorov scale). The filter scale or grid spacing is located within the inertial subrange. All turbulent structures larger than the filter scale are explicitly solved by the model, especially turbulent eddies produced by wind shear, while smaller turbulent structures, i.e. subgrid-scale (SGS) turbulent motions, are modelled through a 1.5-order turbulence closure scheme (amongst others) with the resolution of a SGS turbulent kinetic energy (TKE) conservation equation.

The ARPS momentum and SGS TKE equations have been modified in the same manner as Watanabe (2004) to account for the effect of vegetation on the turbulent flow. As all simulations in this study were performed under dry condition

over a flat terrain, momentum, temperature, pressure and SGS TKE equations presented hereafter are written in Cartesian coordinates for a dry atmosphere, for the sake of simplicity. Despite the fact that the atmosphere is also neutral, the potential temperature equation has been solved in order to activate turbulent motions through initial small turbulent temperature perturbations. Therefore, using the Einstein summation convention, the momentum equation, written for a Boussinesq fluid, is:

$$\bar{\rho}\left(\frac{\partial \tilde{u}_i}{\partial t}+\tilde{u}_j\frac{\partial \tilde{u}_i}{\partial x_j}\right)=-\frac{\partial}{\partial x_i}\left(\tilde{p}''-\alpha_{\mathrm{div}}\frac{\partial \bar{\rho}\tilde{u}_j}{\partial x_j}\right)-2\bar{\rho}\omega_j\epsilon_{ijk}(\tilde{u}_k-\overline{u_k})-\bar{\rho}\,g\left(\frac{\tilde{\theta}''}{\bar{\theta}}-\frac{c_p}{c_v}\frac{\tilde{p}''}{\bar{p}}\right)\delta_{i3}-\frac{\partial \tau_{ij}}{\partial x_j}-\bar{\rho}\,C_d A_f\sqrt{\tilde{u}_j\tilde{u}_j}\tilde{u}_i \tag{1}$$

where the overtilde indicates the filtered variables or grid volume-averaged variables. In this equation, t is time and $x_i(x_1=x, x_2=y, x_3=z)$ refer to the streamwise, lateral, and vertical directions, respectively; $u_i(u_1=u, u_2=v, u_3=w)$ is the instantaneous velocity component along x_i, δ_{ij} is the Kronecker's symbol, ϵ_{ijk} the alternating unit tensor, α_{div} a damping coefficient meant to attenuate acoustic waves, p the air pressure, ρ the air density, g the acceleration due to gravity, θ the potential temperature, c_p and c_v the specific heat of air at constant pressure and volume, respectively.

The terms on the right-hand side of Eq. (1) represent, respectively, the pressure-gradient force term, the Coriolis term, the buoyancy term, the turbulent transport term, and the drag force term induced by the vegetation. In the latter, C_d is the mean drag coefficient of the canopy and A_f is the frontal area density of the vegetation ($m^2\,m^{-3}$).

In the Coriolis term, ω represents the angular velocity of the earth and the second part of the Coriolis term, $-2\bar{\rho}\omega_j\epsilon_{ijk}\overline{u_k}$, represents the geostrophic pressure gradient force associated with the base-state wind. The Coriolis force is only applied on wind perturbations since the steady base state is already geostrophically balanced.

The pressure equation is derived from the equation of state and the mass continuity equation:

$$\frac{\partial \tilde{p}''}{\partial t}+\frac{\partial \tilde{u}_i\,\tilde{p}''}{\partial x_i}=-\bar{\rho}c_s^2\frac{\partial \tilde{u}_i}{\partial x_i}+\bar{\rho}gw \tag{2}$$

where c_s is the full acoustic wave speed. The contribution from diabatic heating is neglected.

The conservation equation for potential temperature writes as follows:

$$\bar{\rho}\left(\frac{\partial \tilde{\theta}''}{\partial t}+\tilde{u}_i\frac{\partial \tilde{\theta}''}{\partial x_i}\right)=-\bar{\rho}w\frac{\partial \bar{\theta}}{\partial z}-\frac{\partial \tau_{i\theta}}{\partial x_i} \tag{3}$$

The Reynolds or subfilter-scale or subgrid stress tensor τ_{ij} is modelled through an SGS eddy-viscosity or gradient-transport model as:

$$\tau_{ij}=-\bar{\rho}\nu_t\left(\frac{\partial \tilde{u}_i}{\partial x_j}+\frac{\partial \tilde{u}_j}{\partial x_i}\right) \tag{4}$$

where ν_t is the eddy viscosity modelled as the product of a length scale l and a velocity scale $\sqrt{e}$ (e being the SGS TKE) characterizing the SGS turbulent eddies:

$$\nu_t=0.1\sqrt{e}l \tag{5}$$

For a neutral atmosphere with isotropic turbulence, the mixing length depends on the grid spacing:

$$l=(\Delta x\,\Delta y\,\Delta z)^{1/3} \tag{6}$$

where Δx, Δy and Δz are the grid spacings in the longitudinal, lateral and vertical directions, respectively. In ARPS, it is also possible to use different horizontal and vertical mixing lengths for various horizontal and vertical grid spacings.

At the surface, the components of the Reynolds stress tensor are defined as:

$$\tau_{i3}|_{\mathrm{surface}}=-\bar{\rho}C_{\mathrm{dm}}\max(V, V_{\mathrm{min}})\tilde{u}_i \tag{7}$$

where $i\in\{1,2\}$, V is the wind velocity at the lowest grid level ($V=\sqrt{\tilde{u_1}^2+\tilde{u_2}^2}|_{\mathrm{surface}}$), V_{min} the lower limit of V, and C_{dm} is the drag coefficient computed in neutral condition from the formulation of Byun (1990).

The conservation equation for the SGS turbulent kinetic energy writes:

$$\frac{\partial e}{\partial t}+\tilde{u}_j\frac{\partial e}{\partial x_j}=-\tau_{ij}\frac{\partial \tilde{u}_i}{\partial x_j}-\frac{g}{\bar{\theta}}\tau_{i\theta}\delta_{i3}+\frac{\partial}{\partial x_j}\left(2\nu_t\frac{\partial e}{\partial x_j}\right)-C_\epsilon\frac{e^{3/2}}{l}-2C_d A_f\sqrt{\tilde{u}_j\tilde{u}_j}e \tag{8}$$

The terms on the right-hand side of Eq. (8) represent, respectively, the dynamic shear production term, the buoyancy production term, the turbulent transport term, the dissipation term and the cascade term for SGS TKE. The latter represents the energy-loss process that accelerates the dissipation of turbulence in the canopy: as the eddies of all scales larger than the canopy elements loose their TKE into both heat and wake through their interaction with vegetation, the inertial eddy-cascade is indeed bypassed (Finnigan, 2000). The production of SGS TKE by wake motions behind vegetation elements is not considered, as their scales are much smaller than those making up the bulk of SGS TKE (Shaw and Schumann, 1992). Furthermore, Shaw and Patton (2003) showed from their LES model using an equation for SGS TKE and another one for the wake kinetic energy that the role of wake motions is essentially to enhance the dissipation of subgrid-scale energy. Wake motions can therefore be simply represented through an increase of the cascade term in a unique SGS TKE conservation equation.

The subgrid heat flux is written as:

$$\tau_{i\theta}=-\bar{\rho}\frac{\nu_t}{Pr}\frac{\partial \tilde{\theta}}{\partial x_i} \tag{9}$$

where Pr is the Prandtl number.

For the sake of clarity the overtilde on $\tilde{u_i}$ will be omitted from now on.

2.2. Numerical details

Three-dimensional simulations were performed over various homogeneous continuous forest canopies within 400 m × 200 m × 200 m domains, corresponding to 200 × 100 × 65 grid points in the x, y and z directions, respectively, with 2 m grid spacing below z = 84 m and a vertically stretched grid above. The forest height is set at 18 m but various frontal area density profiles are considered, depending on the studied cases (see further). The drag coefficient, C_d, is equal to 0.2, which is a usual average value observed for trees. C_d as well as the frontal area density, A_f, are also assumed independent of wind velocity, although Rudnicki et al. (2004) and Vollsinger et al. (2000) observed that the crown frontal area density and drag coefficient of trees may decrease as wind increases since branches and foliage align with wind direction.

The lateral boundary conditions are periodic, the bottom boundaries are treated as rigid and surface momentum flux is parameterized through bulk aerodynamic drag laws (Eq. (7)). A 70 m deep Rayleigh damping layer is used at the upper boundary in order to absorb upward propagating wave disturbances and to eliminate wave reflection at the top of the domain. The velocity fields are initialized from the base-state wind profile (Fig. 1) which was computed from a meteorological pre-processor (Pénelon et al., 2001) with a constant vertical profile of potential temperature (300 K), a dry atmosphere and geostrophic wind components equal to 18.5 m s^{-1} and −3.5 m s^{-1} in the x and y directions, respectively. The flow is driven by the geostrophic pressure gradient associated with the base-state wind in the Coriolis term (Eq. (1)).

2.3. Data analysis

After the flow has reached an equilibrium state, wind velocity and turbulent statistical profiles are computed from a horizontal and time averaging procedure. Horizontal averaging is performed over all x and y locations at each considered z, and time averaging is performed over 90 samples collected for a 30 min period. Consequently, wind velocity components u_i can be decomposed into $u_i = \langle u_i \rangle_{xyt} + u_i'$, where the symbol $\langle\,\rangle_{xyt}$ denotes the time and space average and the prime the deviation from the averaged value.

Zero time-lag two-point correlation coefficients are computed from the velocity components using the following expression:

$$R_{ii}(x,y,z) = \frac{\langle u_i(x,y,z)u_i(0,0,h)\rangle_t}{\sigma_{u_i}(x,y,z)\sigma_{u_i}(0,0,h)} \tag{10}$$

where the reference point is located at the origin of the horizontal coordinates (middle of the computational domain) and at the canopy top, $\sigma_{u_i} = \langle u_i'^2\rangle_t^{1/2}$ is the standard deviation of the wind velocity component u_i. In addition to the time averaging, a spatial averaging is performed on R_{ii} over all x and y locations at each considered z when R_{ii} is analyzed in y−z and x−z planes, respectively.

In order to quantify the respective importance of ejection and sweep motions for the mean momentum flux, their relative contribution and fraction are computed, respectively, as:

$$\Delta S_{0,0} = \frac{\langle u'w'\rangle_{xyt}^{IV} - \langle u'w'\rangle_{xyt}^{II}}{\langle u'w'\rangle_{xyt}} \tag{11}$$

and

$$Q_{uw} = \frac{\langle u'w'\rangle_{xyt}^{IV}}{\langle u'w'\rangle_{xyt}^{II}} \tag{12}$$

where $\langle u'w'\rangle_{xyt}^{IV}$ and $\langle u'w'\rangle_{xyt}^{II}$ are the Reynolds stresses in the fourth (sweeps) and second (ejection) quadrants.

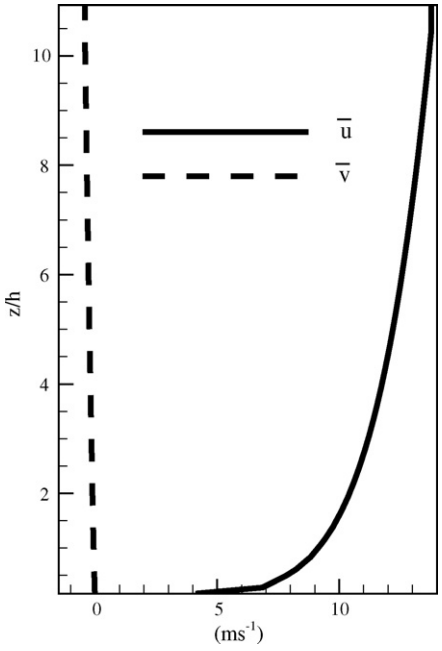

Fig. 1 – Profiles of the horizontal base-state wind velocity components.

3. Model validation

To test our model we use the mean wind velocity and standard turbulent statistics profiles measured by Shaw et al. (1988) within and above a deciduous forest at Camp Borden in Ontario, Canada. These measurements are consistent with others from wind-tunnel and field campaigns (Raupach et al., 1986; Brunet et al., 1994; Kaimal and Finnigan, 1994; Finnigan, 2000), and have already been used by Shaw and Schumann (1992) and Su et al. (1998) to validate their LES models. On top of the turbulent statistics, we also consider turbulent variables such as $\Delta S_{0,0}$, Q_{uw} or R_{ii}. The frontal area density profile used in this validation is shown in Fig. 2 (case 1 with LAI = 2).

3.1. Basic turbulent statistic profiles

Fig. 3a–e shows observed and simulated normalized averaged wind velocity ($\langle u\rangle_{xyt}$), momentum flux ($-\langle u'w'\rangle_{xyt}$), standard deviations of the three wind velocity components ($\sigma_u, \sigma_v, \sigma_w$, where $\sigma_{u_i} = \langle u_i'^2\rangle_{xyt}^{1/2}$), total and SGS TKE ($k_{tot} = 0.5\langle u_i'^2\rangle_{xyt} + \langle e\rangle_{xyt}, \langle e\rangle_{xyt}$), streamwise and vertical velocity skewnesses (Sk_u and Sk_w, where $Sk_{u_i} = \langle u_i'^3\rangle_{xyt}/\langle u_i'^2\rangle_{xyt}^{3/2}$). As can be seen the model performs well for all variables, and with

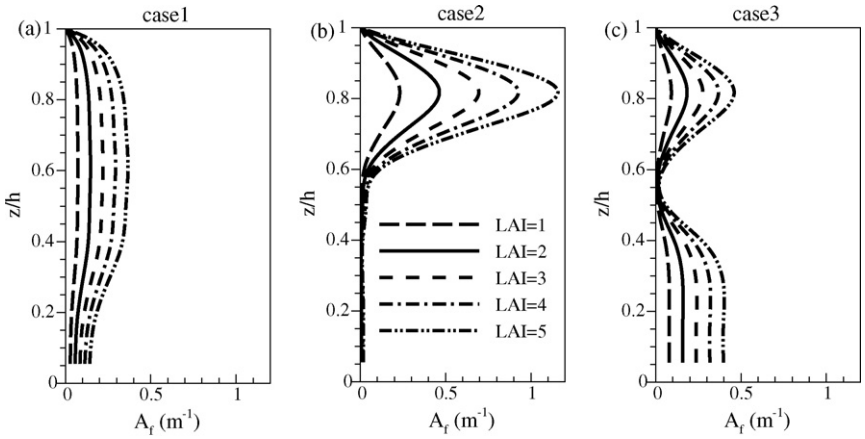

Fig. 2 – Frontal area density profiles for the three types of canopy studied in this paper (cases 1–3), with five values each of leaf-area index (LAI = 1–5).

a similar accuracy as the model of Su et al. (1998). It has to be mentioned that SGS TKE within the canopy only represents less than 10% of total TKE, indicating that flow fields do not strongly depend on the SGS turbulence scheme. Furthermore, the wind velocity profile is logarithmic and the momentum flux is constant above the canopy. The model is, therefore, capable of simulating the constant flux layer although the vertical size of the computational domain does not include the whole atmospheric boundary layer. At canopy top the mean velocity profile is characterized by an inflection point with a strong wind shear. Further down wind velocity decreases exponentially within the canopy as trees extract momentum from the flow through drag forces. The mean wind direction above the canopy follows the base state one (figure not shown) while a swing in wind direction is observed within the canopy, as is observed and discussed in Section 4.1.

Fig. 3f shows the kurtosis of streamwise and vertical velocities, Kt_u and Kt_w (where $Kt_{u_i} = \langle u_i'^4 \rangle_{xyt} / \langle u_i'^2 \rangle^2_{xyt}$), respectively. Within the crown layer, Kt_u peaks at about 3.5 whereas Kt_w increases with depth in the canopy, up to a maximum value of 5 at the ground. Kt_w is always larger than Kt_u. These features indicate the presence of large intermittent eddies that have enough energy to penetrate deep into the canopy. Such behaviour of Kt_u and Kt_w has already been observed by Baldocchi and Meyers (1988) and Green et al. (1995), with somewhat larger values.

In the surface layer the momentum flux is equally controlled by sweep and ejection events (Fig. 3g and h), whereas in the roughness sublayer, around the canopy top, it is dominated by sweeps with maxima in $\Delta S_{0,0}$ and Q_{uw} at about $z = 0.8h$. This feature is in agreement with previous observations (Raupach et al., 1996; Finnigan, 2000; Poggi et al., 2004) and confirms that momentum transfer at canopy top is primarily due to the penetration of the canopy by fast, downward-moving gusts.

The three squared vorticity components $\langle \omega_x \rangle^2_{xyt}$, $\langle \omega_y \rangle^2_{xyt}$, and $\langle \omega_z \rangle^2_{xyt}$ in the streamwise, spanwise and vertical directions, respectively, rapidly decrease in the canopy (Fig. 3i). The spanwise vorticity is maximum at canopy top and larger than the other two components, which indicates that turbulent structures are essentially transverse. Streamwise and vertical vorticities are maximum just above the canopy, at about $z = 1.3h$ and $1.5h$, respectively. These higher positions of $\langle \omega_x \rangle^2_{xyt}$ and $\langle \omega_z \rangle^2_{xyt}$ maxima, compared with $\langle \omega_y \rangle^2_{xyt}$, agrees with the idealized picture of coherent structures proposed by Finnigan (2000) as hairpin-shaped vortical structures or 'double roller' vortices with a downwind tilt from the horizontal. Indeed, the lower base of the double roller vorticies may be characterized by a spanwise vortex at the canopy top, and consequently a maximum in $\langle \omega_y \rangle^2_{xyt}$, while the downwind pair of counter-rotating vortices, characterized by high values of $\langle \omega_x \rangle^2_{xyt}$ and $\langle \omega_z \rangle^2_{xyt}$, are positively inclined from the horizontal. The center of the double roller vortices deduced by Finnigan and Shaw (2000) from their Empirical Orthogonal Function (EOF) analysis is slightly higher ($z = 1.6h$) than our maximum of $\langle \omega_x \rangle^2_{xyt}$. Our averaged vorticity fields account for all types of structures while the EOF analysis allows one to focus only on dominant structures, which probably explains this difference of location.

3.2. *Spatial correlations*

The contours of the correlation for streamwise and vertical velocities, R_{11} and R_{33}, are shown in Figs. 4 and 5, respectively, in the $x-z$, $y-z$ and $x-y$ planes, giving information on the shape and size of coherent structures. As previously observed in wind-tunnel (Shaw et al., 1995), field (Raupach et al., 1991) and LES (Su et al., 2000) experiments, R_{11} has a near-elliptical form in the $x-z$ plane with a downwind tilt from the horizontal. The correlated area (say, $R_{11} > 0.2$) extends from $-3.5h$ to $6h$ in the streamwise direction and over $3.5h$ in the vertical. The downwind tilt of R_{11} is estimated by performing a linear regression on the height of the maximum in R_{11} for each vertical section, from the reference point to the downwind point where R_{11} becomes less than 0.2. The slope angle above the canopy is about 18° and it is smaller within the canopy, in good agreement with previous observations (Shaw et al., 1995).

In the $y-z$ plane, R_{11} is stretched on the vertical with a correlated area extending over $3.5h$ in the vertical and $2h$ in the spanwise direction. Fig. 4c clearly shows the difference in size between the correlated area of the streamwise velocity in the

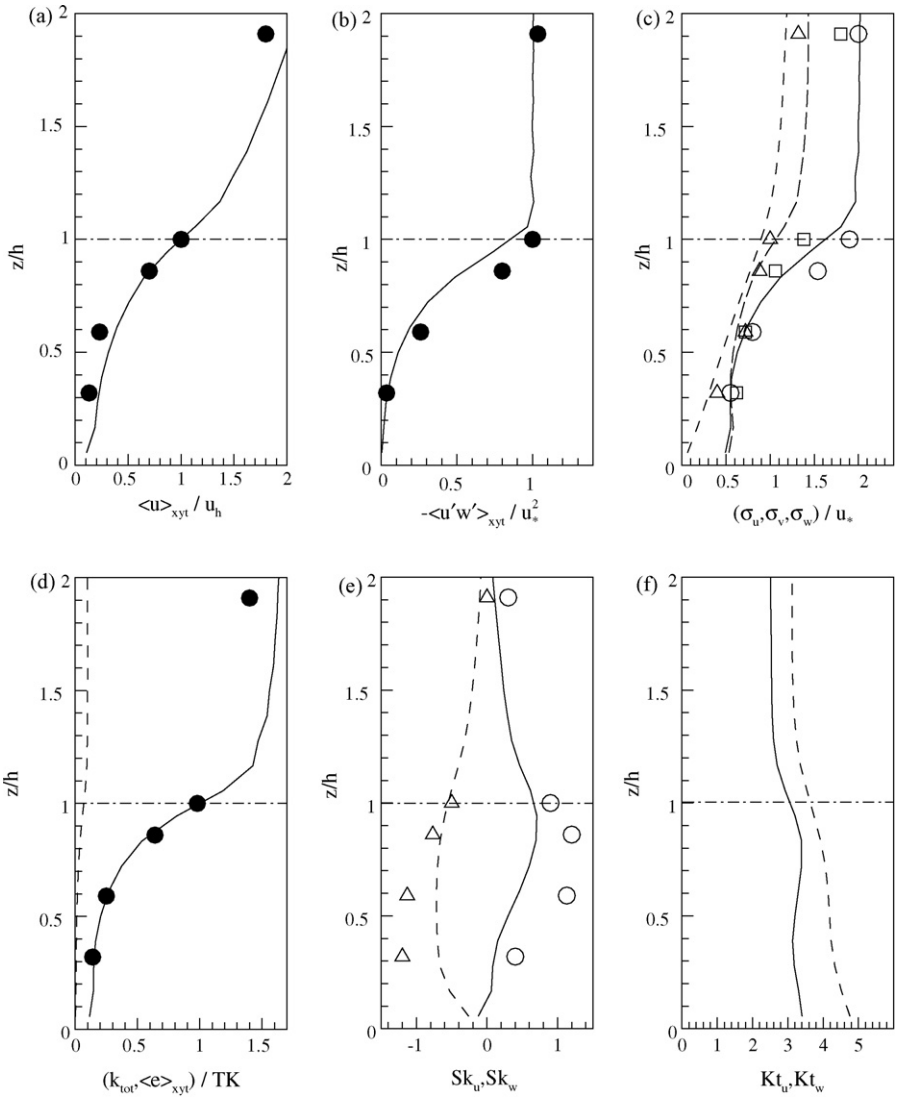

Fig. 3 – Validation of ARPS against the field observations of Shaw et al. (1988) in a homogeneous forest canopy. Comparison between simulated (lines) and observed (symbols) vertical profiles of mean horizontal wind velocity (a); momentum flux (b); standard deviations of the three wind components (c) (σ_u: solid line, empty circle; σ_v: long dashed line, empty square; σ_w: small dashed line, empty triangle); total and SGS TKE (d) (k_{tot}: solid line, symbols; $\langle e \rangle_{xyt}$: dashed line); skewnesses of u and w (e) (Sk_u: solid line, empty circle; Sk_w: dashed line, empty triangle); kurtosis of u and w (f) (Kt_u: solid line; Kt_w: dashed line); relative contribution $\Delta S_{0,0}$ (g) to the momentum flux and fraction Q_{uw} (h) of sweeps and ejections; square of the three vorticity components (i) ($\langle \omega_x \rangle^2_{xyt}$: solid line; $\langle \omega_y \rangle^2_{xyt}$: long dashed line; $\langle \omega_z \rangle^2_{xyt}$: small dashed line). All variables are normalized with the mean streamwise wind velocity at tree top, u_h, and the friction velocity above the canopy, u_*. The experimental dataset is taken from the paper of Su et al. (1998).

streamwise and spanwise directions, with an elongated shape of R_{11} in the former direction.

R_{33} is roughly circular with a diameter of about $2h$ in the three space directions with a slight elongation in the vertical (Fig. 5). The auto-correlation for vertical velocity at mid-canopy height is larger than for the streamwise velocity, the latter decreasing more rapidly with increasing distance from the canopy top.

At mid-canopy ($z = 0.5h$) the maximum of R_{11} occurs with a spatial shift reflecting a positive time delay from the tree top level. This shows that the turbulent structures penetrating into the canopy are inclined in the forward direction. Conversely, the maximum of R_{33} occurs with no time delay, which shows that perturbations in vertical velocity at tree top occur simultaneously at all levels within the canopy. This difference between the time delays of R_{11} and R_{33} within the canopy was also observed from wind-tunnel and in situ measurements by Raupach et al. (1989) and Shaw and Zhang (1992). The latter authors explained that the zero time-lag observed for vertical velocity is due to the rapid diffusion of pressure fluctuations within the canopy, that are essentially created by fluctuations in streamwise velocity at canopy top.

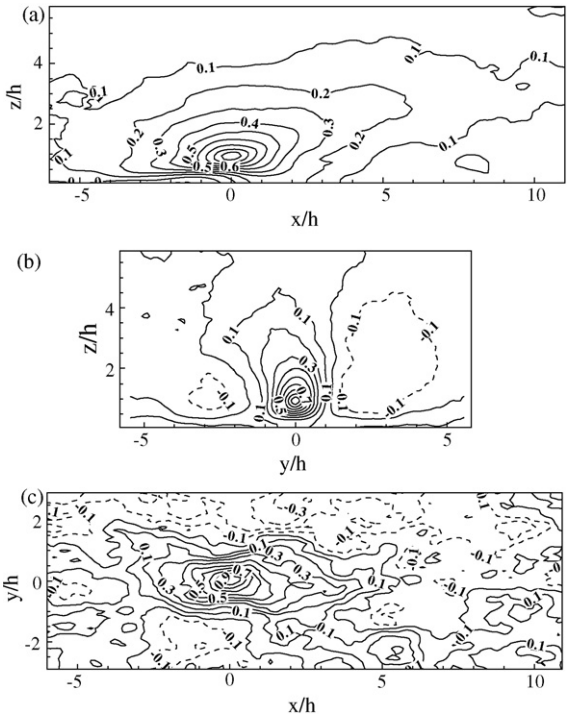

Fig. 4 – Contours of the auto-correlation function for streamwise wind velocity R_{11} in the streamwise (a) and spanwise (b) vertical cross-sections and in the horizontal cross-section at $z = h$ (c).

4. Sensitivity of turbulent statistics to forest morphology

It was shown in the last section that our new version of ARPS is able to reproduce accurately the main features of a turbulent flow within and above a specific, horizontally homogeneous vegetation canopy. We now investigate the sensitivity of the flow to the internal morphology of the canopy. To this purpose, three-dimensional simulations were performed over 15 homogeneous canopies characterized by three types of vertical leaf-area distribution, each with five levels of leaf-area index (LAI = 1–5) as represented in Fig. 2. In case 1, corresponding to that previously studied, the vertical distribution is characterized by a moderate trunk space (Fig. 2a). Case 2 is characterized by a sparse trunk space and a dense crown layer, typical for instance of a Maritime pine (*Pinus pinaster*) stand (Fig. 2b). Case 3 has an upper layer with a (smaller) maximum at the same height as case 2, and an undergrowth in the trunk space, extending vertically up to about 0.35*h* (Fig. 2c).

The recent global synthesis of plant canopy LAI observations performed by Asner et al. (1988) showed that LAI range from 1.3 ± 0.9 for deserts to 8.7 ± 4.3 for tree plantations. Hence, the range of LAI chosen in this study (LAI = 1–5) should provide relevant information on the impact of canopy density variation on turbulent flow fields, without considering extreme cases. The analysis of extreme cases (very sparse and very dense canopies) represents by itself another study that would probably require a different modelling approach in terms of canopy representation, especially for very sparse canopies, and in terms of grid resolution, that would be much more complex and computational time consuming, respectively, than for the intermediate canopy densities used here.

4.1. *Basic turbulent statistic profiles*

Figs. 6–8 present a 'family portrait' of the basic turbulent statistics simulated over the 15 canopies. The overall behaviour of the vertical profiles fits well with that observed in situ and in wind-tunnel by Raupach et al. (1996) (their Fig. 2 a–i), Novak et al. (2000) (Figs. 4 and 5) and Poggi et al. (2004) (Fig. 4), with a similar range of variability and similar sensitivity to the canopy density. Throughout the range of canopy morphology considered here, the turbulent flow at canopy top and above always exhibits the well-known features observed over homogeneous canopies, whereas lower down the canopy morphology induces significant differences.

It can be noticed that the discontinuity of the flow around the canopy top is enhanced with increasing canopy density, and especially with increasing density of the upper canopy as in case 2, which induces a stronger inflection of the streamwise wind profile, slightly larger peaks in Sk_u and Kt_u, and larger wind shear and transverse vorticity. The location of the peak in Sk_u, always between $z = 0.8h$ and $1h$, does not change with increasing canopy density, whereas Poggi et al. (2004) observed it at lower levels, down to $z = 0.5h$, in artificial canopies with vertically homogeneous leaf-area distributions.

Within the canopy, most turbulent variables (wind velocity, momentum flux, uw-correlation ($r_{uw} = \langle u'w' \rangle_{xyt}/\sigma_u\sigma_w$), standard deviation of wind velocity components, vorticity components, skewness of streamwise velocity) get more damped

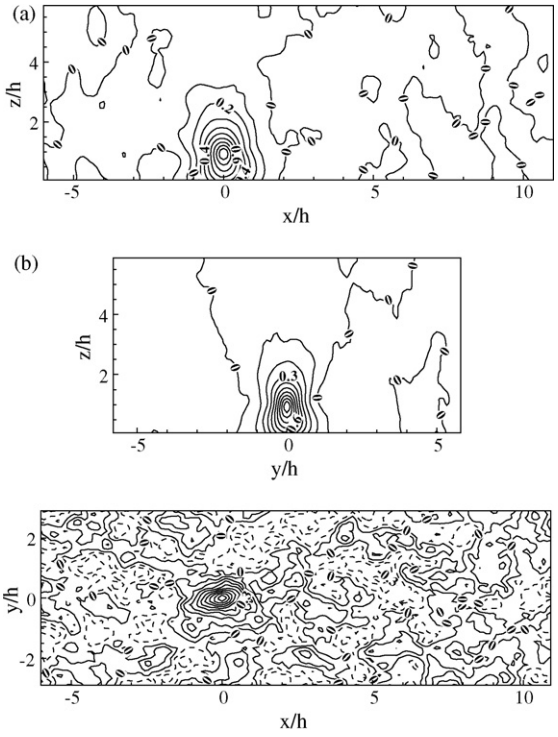

Fig. 5 – Same as Fig. 4, but for the auto-correlation function for vertical wind velocity R_{33}.

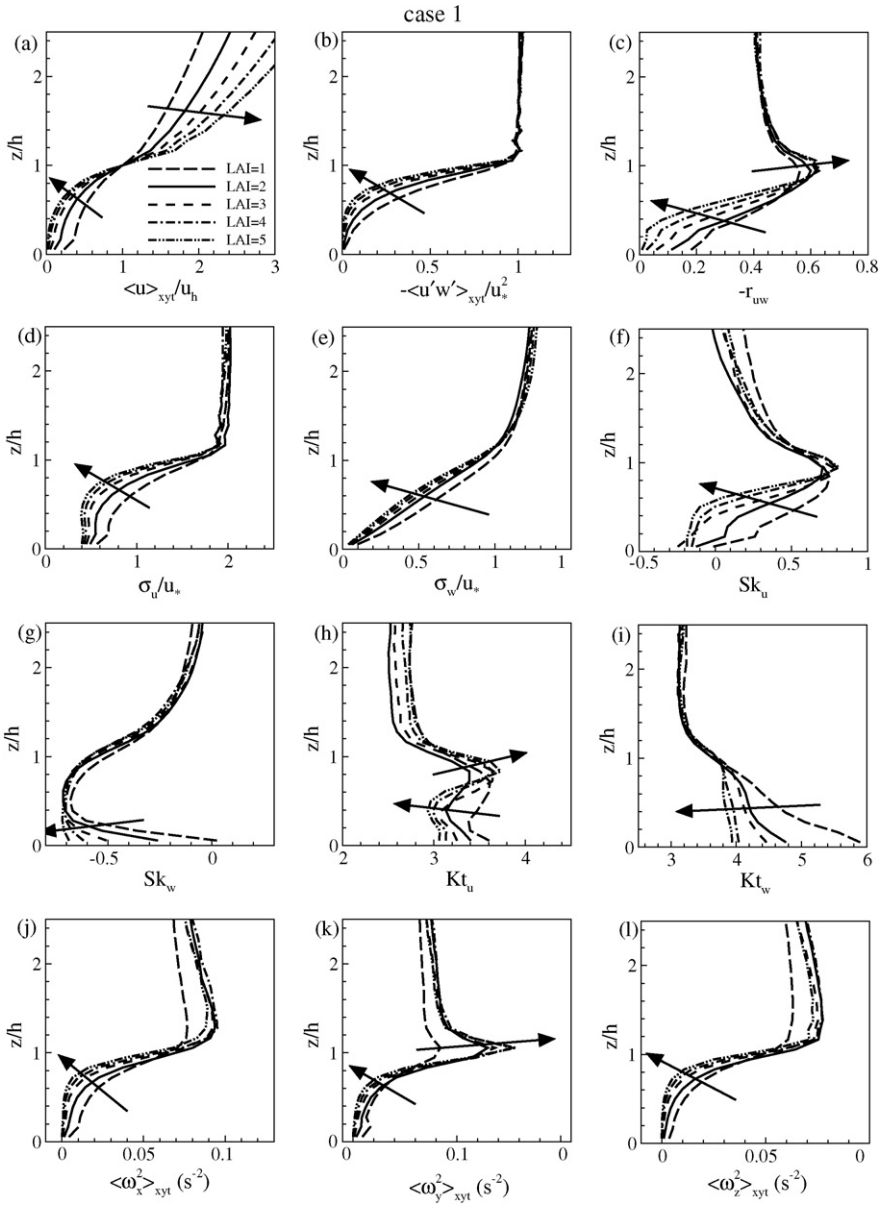

Fig. 6 – Vertical profiles of mean horizontal wind velocity (a), momentum flux (b), *uw* correlation coefficient (c), standard deviations of *u* (d) and *w* (e), skewnesses of *u* (f) and *w* (g), kurtosis of *u* (h) and *w* (i), squared wind vorticity in the *x* (j), *y* (k) and *z* (l) directions, for case 1 canopy with LAI = 1–5 (Fig. 2a). All variables are normalized using the mean streamwise wind velocity at tree top, u_h, and the friction velocity above the canopy, u_*. The arrows show the direction of increasing canopy density.

as density increases, indicating that large intermittent eddies do not have sufficient energy to penetrate deep into the canopy, which is confirmed by the lower maximum of Kt_w. While σ_w profiles are little sensitive to the leaf-area distribution and $\langle u'w' \rangle_{xyt}$ profiles respond only marginally to the density of the upper canopy, the variation of the other variables with depth depends on the vertical foliar distribution. This decrease is stronger within the densest layers of the canopy, while within the sparsest layers variables such as wind velocity $\langle u \rangle_{xyt}$, σ_u and Sk_u slightly increase.

While the wind direction above the canopy is similar to the base state one, the wind direction is modified within the canopy (Fig. 9), especially for the densest canopies, as was also reported by Smith et al. (1972), Kondo and Akashi (1976) and Wilson and Flesch (1999). The swing in wind direction increases with decreasing height and increasing canopy density. At equivalent LAI the swing is the largest in canopies characterized by a dense upper layer and a sparse trunk space (case 2), as was also observed by Kondo and Akashi (1976). The swing across the canopy reaches up to 60° from the canopy top wind direction in case 2 with LAI = 5. However, for the densest canopies, the values of the wind direction in the lower canopy may be taken with caution due to the very low values of the two horizontal wind velocity components, which explain the

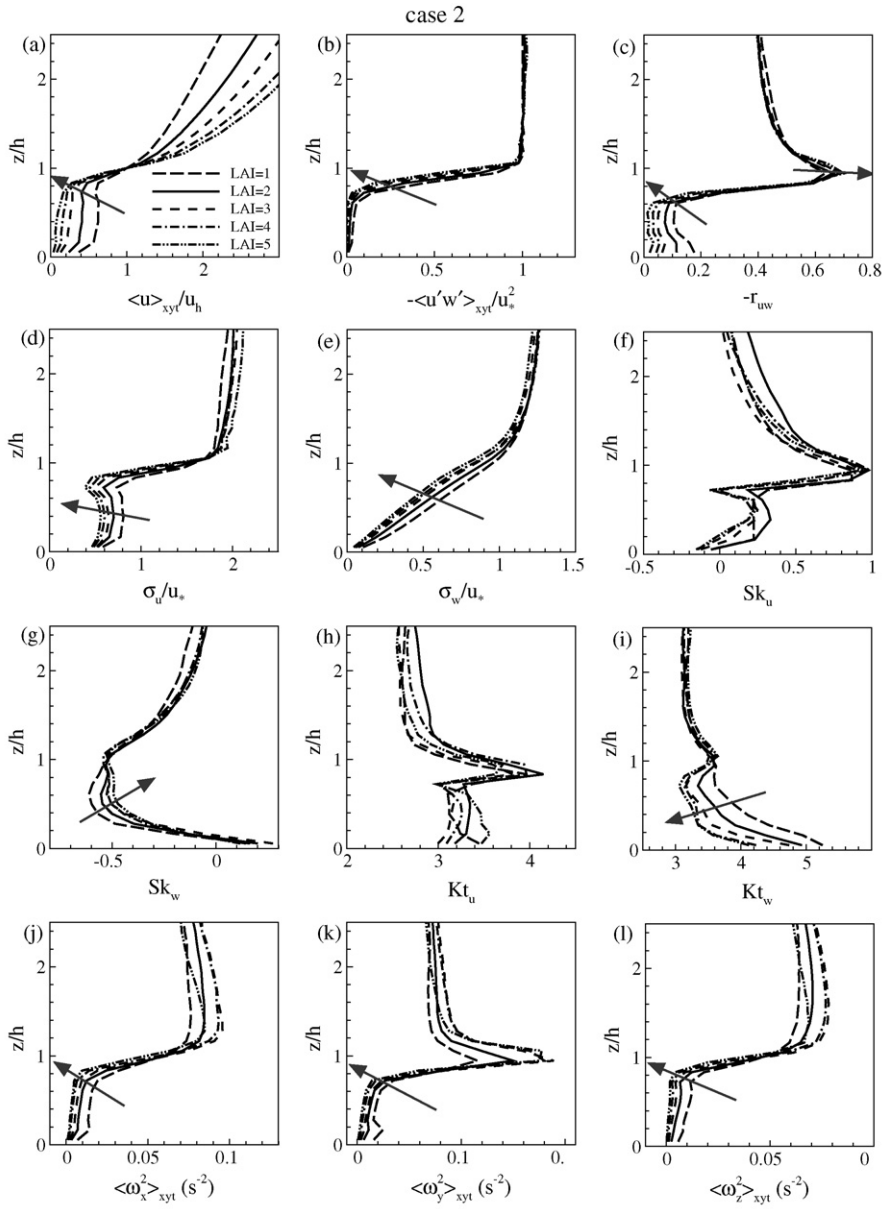

Fig. 7 – Same as Fig. 6 but for case 2 canopies (Fig. 2b).

perturbations visible on wind direction profiles (Fig. 9). This swing in wind direction is caused by an indirect Coriolis effect. As the shear stress gets weak within the canopy, the wind turns so as to align with the large scale pressure gradient which is perpendicular to the geostrophic wind direction at the top of the atmospheric boundary layer.

Fig. 10 shows that the contribution of sweep events to the momentum flux increases with increasing density of the upper canopy: it is larger in case 2 ($Q_{uw} = 1.9$), followed by case 3 ($Q_{uw} = 1.8$) and case 1 ($Q_{uw} = 1.7$). Deeper in the canopy $\Delta S_{0,0}$ responds differently to the leaf-area distribution. In case 1 the sweep contribution decreases, leading to the domination of ejections in the lower half of the canopy for the largest canopy densities, as observed in smooth wall boundary layers (Finnigan and Shaw, 2000). In case 2, ejections strongly dominate the momentum flux just below the crown layer ($z = 0.5h$) with an increasing contribution as the canopy density increases. This sharp change below the crown layer can be seen as resulting from a similar process to what occurs at canopy top, due to a sharp transition between a foliated layer and a very sparse trunk space (but with a lower intensity due to the smaller wind velocity and momentum flux). Within the trunk layer the ejection contribution decreases and becomes equal to that of sweeps close to the ground. In case 3 the sweep contribution decreases within the canopy layer with little vegetation, as in case 2 but to a lesser extent since sweeps remain dominant except for the largest canopy densities. Then, at the top of the undergrowth layer the sweep contribution increases again as it does around the canopy top. Deeper in

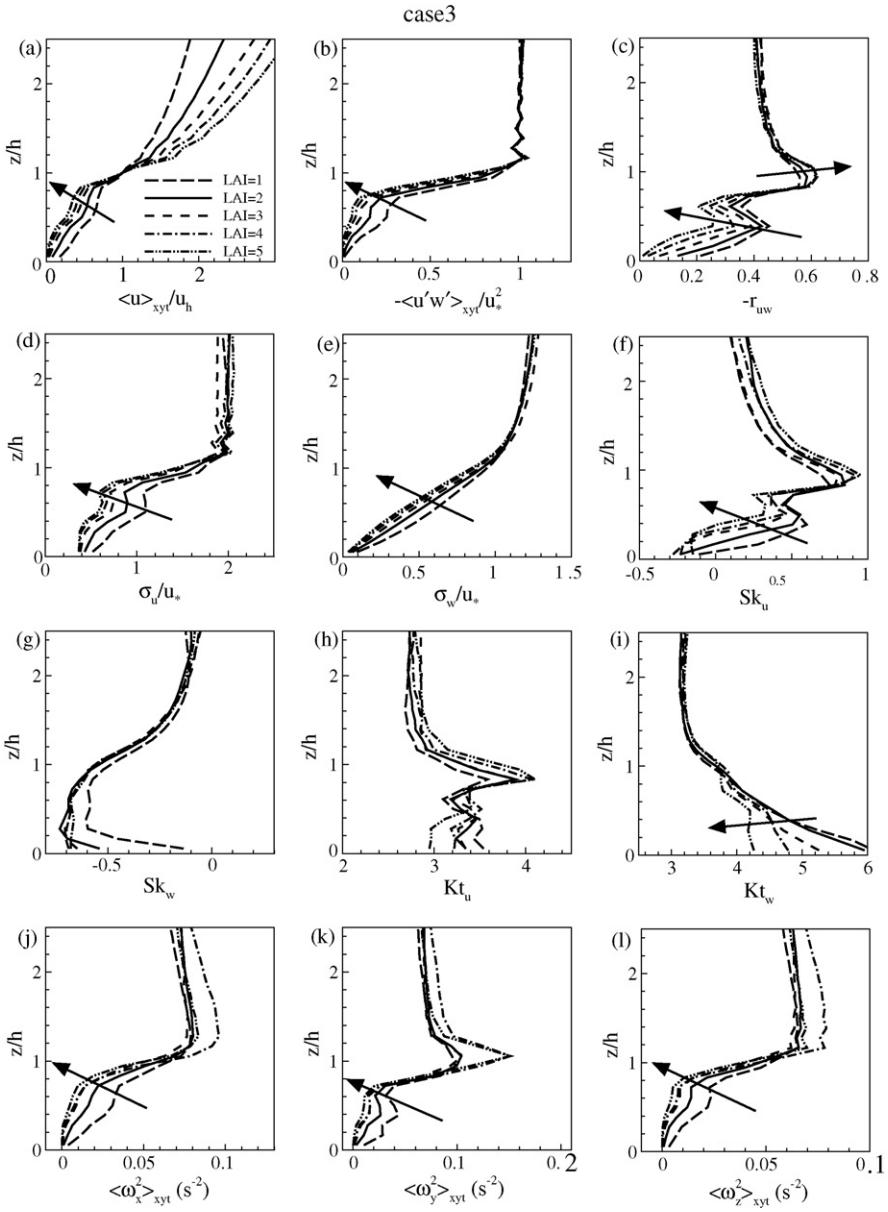

Fig. 8 – Same as Fig. 6 but for case 3 canopies (Fig. 2c).

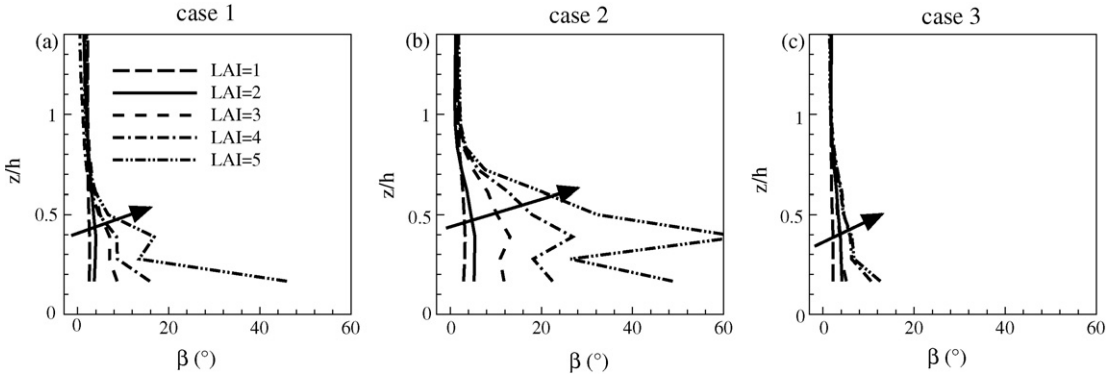

Fig. 9 – Vertical profiles of mean wind direction (β) for the three canopy types (cases 1–3) with LAI = 1–5 (Fig. 2). The arrows show the direction of increasing canopy density.

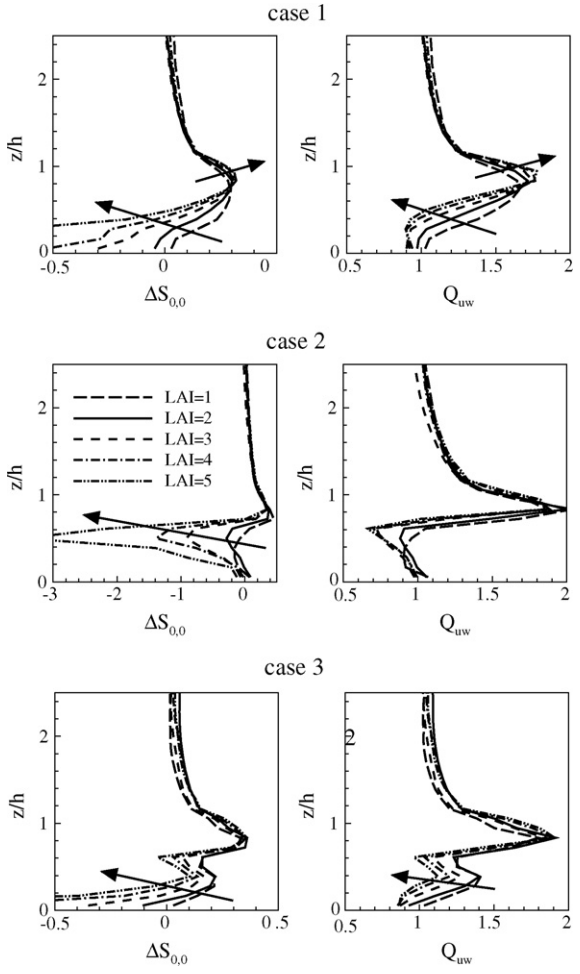

Fig. 10 – Mean vertical variation of the relative contribution ($\Delta S_{0,0}$) to the Reynolds stress and fraction (Q_{uw}) of sweeps and ejections for the three canopy types (cases 1–3) with LAI = 1–5. The arrows show the direction of increasing canopy density.

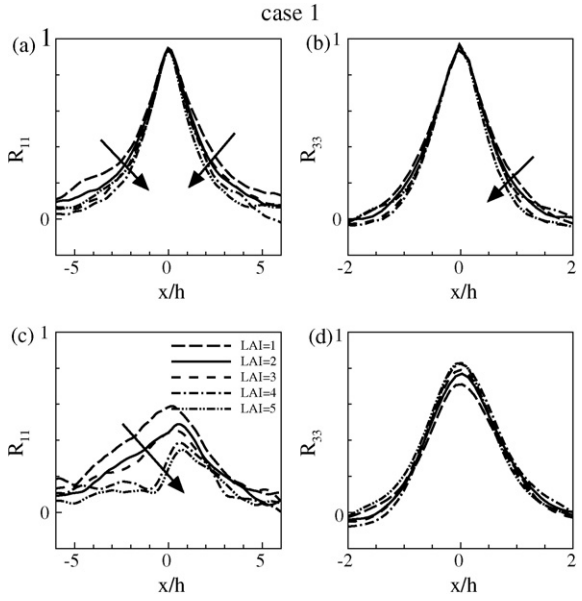

Fig. 11 – Horizontal variation of the average correlation of streamwise (a and c) and vertical (b and d) wind velocities, R_{11} and R_{33}, respectively, at canopy height (a and b) and mid-canopy height (c and d) for case 1 canopies with LAI = 1–5 (Fig. 2a). The arrows show the direction of increasing canopy density.

the undergrowth, ejections become dominant for the densest canopies as observed in case 1.

For the range of canopy densities chosen here, we do not observe the transition of canopy turbulence from a boundary-layer flow (where the momentum flux is controlled by weak ejections) to a mixing-layer flow when the canopy density increases. Such a transition was indeed observed by Poggi et al. (2004) from their wind-tunnel measurements, with much sparser canopies than ours.

4.2. *Spatial correlations*

The contours of the spatial auto-correlations R_{11} and R_{33}, computed for all canopy cases, roughly exhibit the same patterns as those observed in Section 3.2, with an elongated inclined shape in the streamwise direction for R_{11} (not shown). The slope angles of R_{11}, that have been computed for all canopies with the same procedure as that used above, are presented in Table 1. These angles are usually around 18° with lower values when the density of the upper canopy is smaller, i.e. case 1 with LAI = 1 and case 3 with LAI = 1 and 2, probably due to the smaller wind shear above the canopy, which limits the inclination of coherent structures.

Figs. 11–13 illustrate the variability in R_{11} and R_{33} induced by canopy structure, considered here on horizontal streamwise cross-sections at $z = h$ and $z = 0.5h$ (with the reference values at $z = h$). At canopy top, the size of the regions where streamwise and vertical velocities are well-correlated appears little sensitive to canopy density (only in case 1 R_{11} slightly decreases with increasing density). In all cases at mid-canopy, R_{11} clearly decreases with increasing density whereas R_{33} still does not vary much. It is particularly low (and becomes even negative for the largest density) in case 2, where most of the interaction between the flow and the canopy occurs above $z = 0.5h$. The time delay between the two levels that can be deduced from R_{11} (see Figs. 11c, 12c and 13c) increases with the density of the upper canopy. In case 1, it corresponds to a shift in space of about $0.2h$ and $0.7h$ for LAI = 1 and 5, respectively; in case 3, it is about $0.0h$ and $0.4h$ for LAI = 1 and 5, respectively; in case 2, with the largest upper density, it is

Table 1 – Slope angles (°) of the spatial auto-correlation function for streamwise velocity

Case	LAI = 1	LAI = 2	LAI = 3	LAI = 4	LAI = 5
1	14	18	18	18	19
2	20	20	19	20	18
3	12	15	18	20	17

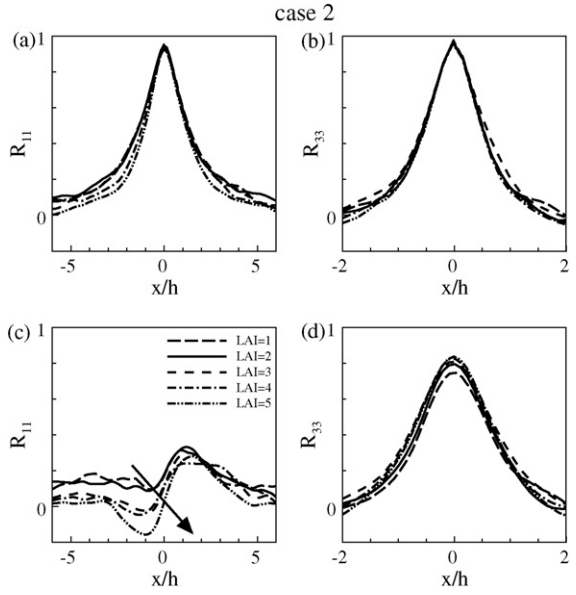

Fig. 12 – Same as Fig. 11 but for case 2 canopies (Fig. 2b).

about $0.8h$ and $1.5h$ for LAI = 1 and 5, respectively. Conversely, the peak in R_{33} occurs at all levels with no time delay in all cases, due to the rapid diffusion of pressure fluctuations within the canopy.

Fig. 14 presents the vertical profiles of R_{11} and R_{33} at $x = 0$. It shows that the sensitivity to canopy density increases with decreasing height and confirms that the correlation decreases with increasing density. All vertical profiles have similar monotonic shapes in the canopy, except for R_{11} in case 2 that shows a minimum at about $z = 0.4h$, before it slightly increases towards the ground; R_{33} is lower there than in the other cases, at least for the largest densities for which the turbulent structures have more difficulty to penetrate into the canopy.

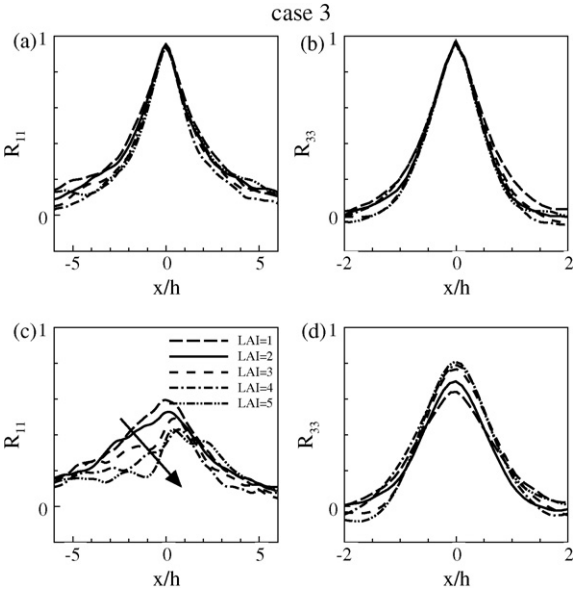

Fig. 13 – Same as Fig. 11 but for case 3 canopies (Fig. 2c).

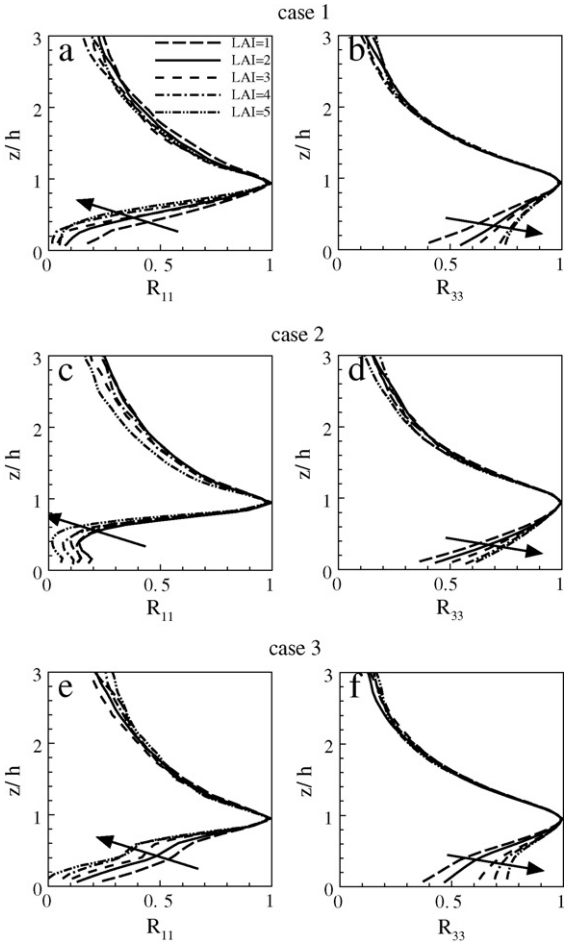

Fig. 14 – Vertical variation (at $x = 0$) of the average correlations of streamwise (R_{11}) and vertical (R_{33}) wind velocities for the three canopy types (cases 1–3) with LAI = 1–5. The arrows show the direction of increasing canopy density.

5. On the analogy of canopy flow with a plane mixing-layer flow

As stated in Section 1, Raupach et al. (1996) established an analogy between a plane mixing layer and the atmospheric flow near the top of a vegetation canopy. This led these authors to express the mean longitudinal separation Λ_w between adjacent coherent structures as a function of a shear length scale L_s defined as $L_s = \langle u \rangle_{xyt}^{z=h} / (\partial \langle u \rangle_{xyt} / \partial z)_{z=h}$. From a series of field and wind-tunnel data they found that $\Lambda_w = mL_s$, with $m \approx 8.1$.

In this section, the validity of this mixing-layer analogy is tested for all 15 canopies studied here. To this purpose, the wavelet transform is used to detect coherent structures in time series of vertical velocity recorded at canopy top in the middle of the computational domain. Scalar time series are usually preferred for this but our simulations were performed in dry, neutral conditions without solving a scalar field. Collineau and Brunet (1993a, b) were the first authors to demonstrate that the wavelet transform is a suitable tool for detecting the dominant turbulent structures in the vicinity of

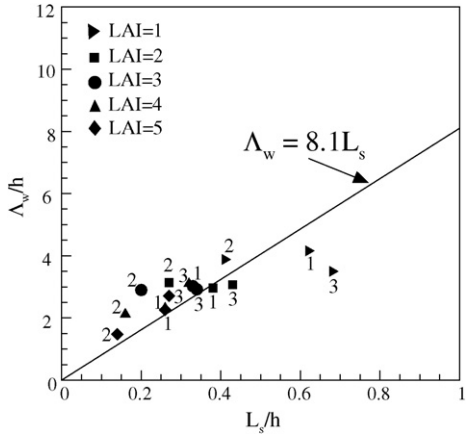

Fig. 15 – Mean streamwise separation Λ_w/h of coherent eddies, plotted against the shear length scale L_s/h for all canopy types and densities considered here. The straight line shows the prediction of Raupach et al. (1996), defined as $\Lambda_w/h = 8.1L_s/h$.

vegetation canopies. Using the same approach, Brunet and Irvine (2000) later confirmed from in situ measurements that $\Lambda_w \approx 8.1L_s$ in neutral condition, and extended this result to non-neutral conditions.

The mean streamwise separation of coherent structures Λ_w is computed for each canopy following a similar procedure as that used by Brunet and Irvine (2000). It is summarized in Appendix A. Λ_w/h is estimated as $(T/N_w)(U_c/h)$, where N_w is the number of structures detected in time T and U_c is the convection velocity of the structures. For the sake of consistency with previous estimates of Λ_w/h we assume that $U_c = 1.8\langle u\rangle_{xyt}^{z=h}$, as was used by Raupach et al. (1996) and observed by Finnigan (1979) and Shaw et al. (1995). Alternately, the convection velocity can be directly deduced from space-time cross-correlations in instantaneous wind fields. However, we chose here to be consistent with the main assumption used by Raupach et al. (1996) to establish a linear relation between Λ_w/h and L_s, in order to find out whether a similar relation, with the same initial assumption, can be observed from our simulations. The analysis of the convection velocity of coherent structures following the canopy morphology is by itself another study that should be the subject of a specific paper.

Fig. 15 shows Λ_w versus the shear length scale L_s, normalized by the canopy height for the 15 canopies considered. The figure also displays the regression line of slope 8.1 obtained by Raupach et al. (1996). As expected, the shear length scale L_s/h increases with decreasing canopy density, from 0.13 for the densest upper canopy layers (case 2 with LAI = 5) to 0.65 for the sparsest (case 3 with LAI = 1). For a given canopy leaf-area index, the shear length scale is also smaller for case 2 canopies, followed by cases 1 and 3; it is therefore mostly controlled by the density of the upper canopy layer.

Our results are consistent with (although slightly above than) the regression line from Raupach et al. (1996), to the exception of the canopies with a very sparse upper layer (cases 1 and 3 with LAI = 1), in which case the data points tend to fall below the regression line. A regression analysis of our data, discarding cases 1 and 3 with LAI = 1, results in a slope equal to 8.7, which is close to 8.1 obtained by Raupach et al. (1996). The discrepancy of the two canopies with very sparse upper layer from the regression line was also observed by Novak et al. (2000) with the sparsest tree canopies they used in a wind-tunnel. This implies that for a given wind profile (i.e. a given L_s) the mean streamwise separation between adjacent coherent structures is smaller than that predicted by the regression of Raupach et al. (1996). This difference in the behaviour of turbulent flows over sparse canopies is probably due to the fact that the inflection in the mean horizontal velocity becomes too weak to sustain the instability process responsible for the generation of mixing-layer eddies. With less vegetation the canopy flow progressively evolves towards a boundary layer flow. As mentioned previously, this can also be inferred from the wind-tunnel measurements of Poggi et al. (2004), who used a larger range of densities than ours.

6. Summary

The atmospheric model ARPS has been modified to simulate turbulent flows at fine scale over vegetation canopies with a large-eddy simulation approach. This new version of ARPS has been validated successfully in the case of a homogeneous canopy by looking at profiles of turbulent statistics such as mean wind velocity, turbulent kinetic energy, momentum flux and velocity skewnesses, as well as spatial velocity correlations. This validation has shown that the model is able to reproduce accurately the main observed features of turbulent canopy flows.

A sensitivity study of the turbulent flow to the morphology of the canopy, i.e. the density and the vertical leaf-area distribution, has then been performed over 3 types of canopy with 5 levels of leaf-area index, from 1 to 5. The simulations have been able to reproduce the 'universal' characteristics of canopy flows and have provided a quantification of the impact of vegetation density on these characteristics. The resulting scatter in the vertical profiles is similar to the residual variability than can be observed on experimental wind-tunnel and in situ data, when plotted in the same non-dimensional format (Raupach et al., 1996; Novak et al., 2000).

The typical features of canopy flow become more pronounced as canopy density increases: (i) turbulent variables such as turbulent kinetic energy and momentum flux decrease more rapidly with depth, as coherent structures have more difficulty to penetrate into the canopy; (ii) the swing in wind direction into the canopy increases with decreasing height; (iii) the contribution of sweeps to the momentum flux at canopy top increases; (iv) the streamwise and, to a lesser extent, the vertical wind velocity components are well correlated in a smaller longitudinal region; and (v) the turbulent structures penetrating into the canopy tend to be more inclined. For a given canopy leaf-area index, the vertical leaf-area distribution also plays a significant role, in the sense that the density of the upper canopy exert a major influence on the turbulent flow. In the extreme case of a dense upper foliated layer above a sparse trunk space (case 2 with large LAI), we even observed that on the lower side of the vegetation layer the momentum flux becomes dominated by ejections whereas sweeps prevail on the upper side.

The mean streamwise separation Λ_w between adjacent coherent structures at canopy top has been computed from wavelet transform techniques for each canopy with the same assumption on the convection velocity as used by Raupach et al. (1996). For canopies with LAI > 1, we observed a clear relationship between Λ_w and the shear length scale L_s, close to that predicted by the mixing-layer analogy proposed by Raupach et al. (1996) and confirmed by wind-tunnel and field measurements. However, for the sparsest canopies (LAI = 1) Λ_w is smaller than the predicted value. With decreasing canopy density, the turbulent flow may evolve from a typical mixing layer towards a rough-wall boundary layer. However, the LAI range used here is probably too narrow to observe this transition, that may be better inferred from the wind-tunnel measurements of Poggi et al. (2004).

Only homogeneous canopies have been considered in this paper. However companion, forthcoming papers will present a validation of the model across a simple forest-clearing-forest pattern (Dupont and Brunet, 2008), and analyze the development of coherent structures from the leading edge of the forest (Dupont and Brunet, 2008, in press, s).

Acknowledgements

We would like to thank the Center for Analysis and Prediction of Storms (CAPS) at the University of Oklahoma for providing the ARPS code. Computer simulations related to this work were performed on the EPHYSE cluster and on the NEC-SX8 at the Institut du Développement et des Ressources en Informatique Scientifique (IDRIS), Orsay, France. Thanks are expressed to Patrick Moreau, Tovo Rabemanantsoa, Guy Pracros and Dr. Mark R. Irvine for their help with the cluster setup. Dr. Mark R. Irvine is also gratefully acknowledged for his help on the wavelet transform tool. We would like to thank the GIP Ecofor for its financial support through the ''Fort, vent et risques'' programme that funded the Venfor project. Finally, we thank an anonymous reviewer for his/her helpful comments.

Appendix A. Ramp-signal detection with wavelet transform

In order to detect coherent structures in time series, as occasional large excursions from the mean, we use the wavelet transform following the same approach as that used by Collineau and Brunet (1993a, b) and Brunet and Irvine (2000). Unlike the Fourier Transform, the wavelet transform unfolds turbulent variable time series into both time (or space) and scale. The continuous wavelet transform of a signal, $h(t)$, is defined as:

$$T_p(a,b) = \frac{1}{a^p}\int_{-\infty}^{\infty} h(t)g\left(\frac{t-b}{a}\right)\mathrm{d}t, \tag{A.1}$$

where $g(t)$ is the wavelet function, a the wavelet scale, b the position translation, p a normalization factor taken as 1 here, and $T_p(a,b)$ represents the wavelet coefficients.

As the normalized wavelet variance spectrum $W_p(a)$ represents the distribution of energy along the scales (or wavelet dilatation) a, its peak can be interpreted as showing the scale of coherent structures. The variance spectrum is given as:

$$W_p(a) = \int_{-\infty}^{\infty} |T_p(a,b)|^2 \mathrm{d}b. \tag{A.2}$$

Since no scalar field is simulated here, the wavelet transform is applied on time series of instantaneous vertical velocity with the following methodology.

- Wavelet transforms are computed from Haar wavelet over 30-min data runs simulated by the model at canopy top in the middle of the computational domain, and sampled at 33 Hz.
- The representative scale of coherent structures is deduced from the wavelet variance spectra (peak scale).
- Since the Mhat detection function crosses zero when a coherent structure is detected (Collineau and Brunet, 1993b), the previous Haar peak scale is converted into the corresponding Mhat scale, and wavelet coefficients are calculated with the characteristic scale of coherent structures, using the Mhat wavelet.
- The number of 'zero crosses' in the detection function is then counted to determine the average temporal separation of coherent structures in the total time period, and their frequency is deduced. Similarly to Barthlott et al. (2007), zero-crossings whose corresponding maximum is at least lower than 10% of the maximum of wavelet coefficients are not counted as coherent structures.
- Coherent eddy separation Λ_w, normalized by canopy height h, is then calculated by approximating the convection velocity U_c of coherent structures to 1.8 times the average wind velocity at the canopy top (as has been observed by Finnigan (1979) and Shaw et al. (1995), and is often used (Raupach et al., 1996)):

$$\frac{\Lambda_w}{h} = \frac{TU_c}{N_w h} \tag{A.3}$$

where T is the total duration of the time series and N_w is the number of events identified in the w time series by the Mhat detection function.

REFERENCES

Asner, G.P., Scurlock, J.M.O., Hicke, J.A., 1988. Global synthesis of leaf area index observations: implications for ecological and remote sensing studies. Global Ecol. Biogeogr. 12, 191–205.
Baldocchi, D., Meyers, T.P., 1988. Turbulence structure in a deciduous forest. Boundary-Layer Meteorol. 43, 345–364.
Barthlott, C., Drobinski, P., Fesquet, C., Dubos, T., Pietras, C., 2007. Long-term study of coherent structures in the atmospheric surface layer. Boundary-Layer Meteorol. 125, 1–24.
Brunet, Y., Finnigan, J.J., Raupach, M.R., 1994. A wind tunnel study of air flow in waving wheat: single-point velocity statistics. Boundary-Layer Meteorol. 70, 95–132.
Brunet, Y., Irvine, M.R., 2000. The control of coherent eddies in vegetation canopies: streamwise structure spacing, canopy shear scale and atmospheric stability. Boundary-Layer Meteorol. 94, 139–163.

Byun, D.W., 1990. On the analytical solutions of flux-profile relationships for the atmospheric surface layer. J. Appl. Meteorol. 29, 652–657.
Collineau, S., Brunet, Y., 1993a. Detection of turbulent coherent motions in a forest canopy. Part I. Wavelet analysis. Boundary-Layer Meteorol. 65, 357–379.
Collineau, S., Brunet, Y., 1993b. Detection of turbulent coherent motions in a forest canopy. Part II. Timescales and conditional averages. Boundary-Layer Meteorol. 66, 49–73.
Dupont, S., Brunet, Y., 2008. Edge flow and canopy structure: a large-eddy simulation study. Boundary-Layer Meteorol. 126, 51–71.
Dupont, S., Brunet, Y. Impact of forest edge shape on tree stability: a large-eddy simulation study. Forestry, in press.
Dupont, S., Brunet, Y., 2008b. Coherent structures in canopy edge flow: a large-eddy simulation study. J. Fluid Mech., submitted for publication.
Dwyer, M.J., Patton, E.G., Shaw, R.H., 1997. Turbulent kinetic energy budgets from large-eddy simulation of airflow above and within a forest canopy. Boundary-Layer Meteorol. 84, 23–43.
Finnigan, J.J., 1979. Turbulence in waving wheat. II. Structure of momentum transfer. Boundary-Layer Meteorol. 16, 223–236.
Finnigan, J.J., 2000. Turbulence in plant canopies. Annu. Rev. Fluid Mech. 32, 519–571.
Finnigan, J.J., Shaw, R.H., 2000. A wind-tunnel study of airflow in waving wheat: an EOF analysis of the structure of the large-eddy motion. Boundary-Layer Meteorol. 96, 211–255.
Gao, W., Shaw, R.H., Paw U, K.T., 1989. Observation of organised structures in turbulent flow within and above a forest canopy. Boundary-Layer Meteorol. 47, 349–377.
Green, S.R., Grace, J., Hutchings, N.J., 1995. Observations of turbulent air flow in three stands of widely spaced sitka spruce. Agric. For. Meteorol. 74, 205–225.
Kaimal, J.C., Finnigan, J.J., 1994. Atmospheric Boundary Layer Flows. Their Structure and Measurements. Oxford University Press, New York, p. 289.
Kanda, M., Hino, M., 1994. Organized structures in developing turbulent flow within and above a plant canopy, using a large eddy simulation. Boundary-Layer Meteorol. 68, 237–257.
Kondo, J., Akashi, S., 1976. Numerical studies on the two-dimensional flow in horizontally homogeneous canopy layers. Boundary-Layer Meteorol. 10, 255–272.
Lu, C.H., Fitzjarrald, D.R., 1994. Seasonal and diurnal variations of coherent structures over a deciduous forest. Boundary-Layer Meteorol. 69, 43–69.
Novak, M.D., Warland, J.S., Orchansky, A.L., Ketler, R., Green, S., 2000. Wind tunnel and field measurements of turbulent flow in forests. Part I. Uniformly thinned stands. Boundary-Layer Meteorol. 95, 457–495.
Patton, E.G., Shaw, R.H., Judd, M.J., Raupach, M.R., 1998. Large-eddy simulation of windbreak flow. Boundary-Layer Meteorol. 87, 275–306.
Poggi, D., Porporato, A., Ridolfi, L., Albertson, J.D., Katul, G.G., 2004. The effect of vegetation density on canopy sub-layer turbulence. Boundary-Layer Meteorol. 111, 565–587.
Pénelon, T., Calmet, I., Mironov, D.V., 2001. Micrometeorological simulations over a complex terrain with SUBMESO: a model study using a novel pre-processor. Int. J. Environ. Pollut. 16, 583–602.
Raupach, M.R., Coppin, P.A., Legg, B.J., 1986. Experiments on scalar dispersion within a model plant canopy. Part I. The turbulence structure. Boundary-Layer Meteorol. 35, 21–52.
Raupach, M.R., Finnigan, J.J., Brunet, Y., 1989. Coherent eddies in vegetation canopies. In: Proceedings of the Fourth Australian Conference on Heat and Mass Transfer, Christchurch, NZ, 9–12 May 1989, pp. 75–90.
Raupach, M.R., Antonia, R.A., Rajagopalan, S., 1991. Rough-wall turbulent boundary layers. Appl. Mech. Rev. 44, 1–25.
Raupach, M.R., Finnigan, J.J., Brunet, Y., 1996. Coherent eddies and turbulence in vegetation canopies: the mixing-layer analogy. Boundary-Layer Meteorol. 78, 351–382.
Rudnicki, M., Mitchell, S.J., Novak, M.D., 2004. Wind tunnel measurements of crown streamlining and drag relationships for three conifer species. Can. J. For. Res. 34, 666–676.
Shaw, R.H., Hartog, D., Neumann, H.H., 1988. Influence of foliar density and thermal stability on profiles of Reynolds stress and turbulence intensity in a deciduous forest. Boundary-Layer Meteorol. 45, 391–409.
Shaw, R.H., Schumann, U., 1992. Large-eddy simulation of turbulent flow above and within a forest. Boundary-Layer Meteorol. 61, 47–64.
Shaw, R.H., Zhang, X.J., 1992. Evidence of pressure-forced turbulent flow in a forest. Boundary-Layer Meteorol. 58, 273–288.
Shaw, R.H., Brunet, Y., Finnigan, J.J., Raupach, M.R., 1995. A wind tunnel study of air flow in waving wheat: two-point velocity statistics. Boundary-Layer Meteorol. 76, 349–376.
Shaw, R.H., Patton, E.G., 2003. Canopy element influences on resolved- and sub-grid-scale energy within a large-eddy simulation. Agric. For. Meteorol. 115, 5–17.
Shen, S., Leclerc, M.Y., 1997. Modelling the turbulence structure in the canopy layer. Agric. For. Meteorol. 87, 3–25.
Smith, F.B., Carson, D.J., Oliver, H.R., 1972. Mean wind-direction shear through a forest canopy. Boundary-Layer Meteorol. 3, 178–190.
Su, H.-B., Shaw, R.H., Paw U, K.T., Moeng, C.-H., Sullivan, P.P., 1998. Turbulent statistics of neutrally stratified flow within and above a sparse forest from large-eddy simulation and field observations. Boundary-Layer Meteorol. 88, 363–397.
Su, H.-B., Shaw, R.H., Paw U, K.T., 2000. Two-point correlation analysis of neutrally stratified flow within and above a forest from large-eddy simulation. Boundary-Layer Meteorol. 94, 423–460.
Vollsinger, S., Mitchell, S.J., Byrne, K.E., Novak, M.D., Rudnicki, M., 2000. Wind tunnel measurements of crown streamlining and drag relationships for several hardwood species. Can. J. For. Res. 35, 1238–1249.
Watanabe, T., 2004. Large-eddy simulation of coherent turbulence structures associated with scalar ramps over plant canopies. Boundary-Layer Meteorol. 112, 307–341.
Wilson, J.D., Flesch, T.K., 1999. Wind and remnant tree sway in forest cutblocks. III. A windflow model to diagnose spatial variation. Agric. For. Meteorol. 93, 259–282.
Xue, M., Droegemeier, K.K., Wong, V., Shapiro, A., Brewster K., 1995. ARPS Version 4.0 User's Guide. Center for Analysis and Prediction of Storms, University of Oklahoma, Norman, OK, p. 380.
Xue, M., Droegemeier, K.K., Wong, V., 2000. The Advanced Regional Prediction System (ARPS)–A multi-scale nonhydrostatic atmospheric simulation and prediction model. Part I. Model dynamics and verification. Meteorol. Atmos. Phys. 75, 161–193.
Xue, M., Droegemeier, K.K., Wong, V., Shapiro, A., Brewster, K., Carr, F., Weber, D., Liu, Y., Wang, D., 2001. The Advanced Regional Prediction System (ARPS)–A multi-scale nonhydrostatic atmospheric simulation and prediction tool. Part II. Model physics and applications. Meteorol. Atmos. Phys. 76, 143–165.
Yang, B., Raupach, M., Shaw, R.H., Paw U, K.T., Morse, A.P., 2006a. Large eddy simulation of turbulent flow across a forest edge. Part I. Flow statistics. Boundary-Layer Meteorol. 120, 377–412.
Yang, B., Morse, A.P., Shaw, R.H., Paw U, K.T., 2006b. Large eddy simulation of turbulent flow across a forest edge. Part II. Momentum and turbulence kinetic energy budgets. Boundary-Layer Meteorol. 121, 433–457.